GA–A24850

ONSET AND SUPPRESSION OF 2/1 NTM IN DIII–D

by
C.C. PETTY, D.P. BRENNAN, T.C. LUCE, R.J. LA HAYE, D.A. HUMPHREYS,
J.R. FERRON, I.A. GORELOV, A.W. HYATT, K. KAJIWARA, S.E. KRUGER,
L.L. LAO, J. LOHR, F.W. PERKINS, P.A. POLITZER, R. PRATER,
D.D. SCHNACK, E.J. STRAIT, A.D. TURNBULL, M.R. WADE,
and A.S. WELANDER

OCTOBER 2004

DISCLAIMER

GA–A24850

ONSET AND SUPPRESSION OF 2/1 NTM IN DIII–D

by
C.C. PETTY, D.P. BRENNAN,* T.C. LUCE, R.J. LA HAYE, D.A. HUMPHREYS, J.R. FERRON, I.A. GORELOV, A.W. HYATT, K. KAJIWARA,† S.E. KRUGER,‡ L.L. LAO, J. LOHR, F.W. PERKINS,Δ P.A. POLITZER, R. PRATER, D.D. SCHNACK,# E.J. STRAIT, A.D. TURNBULL, M.R. WADE,∞ and A.S. WELANDER

This is a preprint of a paper to be presented at the 20th IAEA Fusion Energy Conference, Vilamoura, Portugal, November 1–6, 2004 and to be published in the *Proceedings.*

*Massachusetts Institute of Technology, Cambridge, Massachusetts.
†Oak Ridge Institute for Science Education, Oak Ridge, Tennessee.
‡Tex-X, Boulder, Colorado.
ΔPrinceton Plasma Physics Laboratory, Princeton, New Jersey.
#SAIC, San Diego, California.
∞Oak Ridge National Laboratory, Oak Ridge, Tennessee.

Work supported by
the U.S. Department of Energy
under DE-FC02-04ER54698, DE-AC05-76OR00033,
DE-AC02-76CH03073, and DE-AC05-00OR22725

GENERAL ATOMICS PROJECT 30200
OCTOBER 2004

Onset and Suppression of 2/1 NTM in DIII-D

C.C. Petty,[1] D.P. Brennan,[2] T.C. Luce,[1] R.J. La Haye,[1] D.A. Humphreys,[1] J.R. Ferron,[1] I.A. Gorelov,[1] A.W. Hyatt,[1] K. Kajiwara,[3] S.E. Kruger,[4] L.L. Lao,[1] J. Lohr,[1] F.W. Perkins,[5] P.A. Politzer,[1] R. Prater,[1] D.D. Schnack,[6] E.J. Strait,[1] A.D. Turnbull,[1] M.R. Wade.[7] and A.S. Welander

[1]General Atomics, P.O. Box 85608, San Diego, California 92186-5608, USA
[2]Massachusetts Institute of Technology, Cambridge,Massachusetts, USA
[3]Oak Ridge Institute for Science Education, Oak Ridge, Tennessee, USA
[4]Tex-X, Boulder, Colorado, USA
[5]Princeton Plasma Physics Laboratory, Princeton, New Jersey, USA
[6]SAIC, San Diego, California, USA
[7]Oak Ridge National Laboratory, Oak Ridge, Tennessee, USA

e-mail contact of main author: petty@fusion.gat.com

Abstract. Complete suppression of the important $m = 2/n = 1$ neoclassical tearing mode (NTM) has been achieved recently in DIII-D using electron cyclotron current drive (ECCD) in the island O-point. High performance, hybrid-regime discharges were used with $\beta_N \approx 2.8$ ($\beta \approx 3.5\%$), which equals 90% of the ideal kink no-wall stability limit. Using up to 3.0 MW of unmodulated power to drive up to 40 kA of ECCD at $\rho = 0.67$ (the location of the $q = 2$ surface), the $m = 2/n = 1$ NTM was stabilized resulting in a ≈30% improvement (recovery) of the energy confinement time. Recent developments in the theory of NTMs have enabled us to identify the observed islands as being classically destabilized with $\Delta' > 0$. This was done in experiments by varying the heating rate $d\beta/dt$ prior to onset and comparing the resulting island growth rate to a comprehensive model. The time dependence of Δ' as β increased was a critical physics element along with neoclassical and polarization effects. The theory predicts transitions at different heating rates for onset of classical modes, seeded NTMs, and ideal modes. These were in agreement with the modes observed.

1. Introduction

Optimal operation of tokamak plasmas requires the consideration of stability limits for tearing modes, which can be substantially lower than the ideal MHD pressure limit. In the zero pressure limit, tearing modes are driven by the free energy in the poloidal magnetic field [1,2]. The stability of this classical tearing mode is governed by the linear stability index Δ', which represents the change in free energy caused by the tearing mode perturbation. When $\Delta' > 0$, the mode is unstable. For a finite pressure gradient, the deficit in the bootstrap current density caused by a flattening of the pressure gradient in the O-point of the island can give rise to a neoclassical tearing mode (NTM) [3,4]. NTMs are typically linearly stable ($\Delta' < 0$) but nonlinearly unstable and require a finite seed island to grow. The seed island can be generated by forced reconnection from a fluctuation in the plasma or by the classical destabilization of a tearing mode at a rational surface. All finite β tearing modes become NTMs after the initial linear phase; therefore, the classical and neoclassical tearing modes need to be considered in a common framework.

The important $m = 2/n = 1$ NTM, in addition to reducing the energy confinement time, can lock to the vessel wall, rapidly grow, and lead to a plasma disruption. Here m is the poloidal mode number and n is the toroidal mode number for tearing modes resonant at safety factor $q = m/n$. The onset and suppression of the $m = 2/n = 1$ NTM have been studied in separate experiments in the DIII-D tokamak. A new theoretical framework for understanding the variety of tearing mode phenomena in DIII-D has been recently developed. One key to this model is the inclusion of the dynamic dependence of the linear drive Δ' due to changing equilibrium conditions. This provides a framework for understanding the range of tearing phenomena in terms of the interactive dynamics of equilibrium, stability, and transport under external driving factors, which yields a range of dynamical solutions in agreement with experiment. The NTM has two important drive mechanisms — the Δ' linear drive and the

neoclassical bootstrap current. Two strategies exist for active stabilization. One can either replace the "missing" bootstrap current within the island [5,6], or modify Δ' to make it more negative. Electron cyclotron current drive (ECCD) is a prime candidate for both methods, and complete suppression of the $m = 2/n = 1$ NTM by ECCD has been demonstrated already in DIII-D [7] and ASDEX Upgrade [8]. The unmodulated ECCD suppression results reported here extend the previous work by stabilizing the $m = 2/n = 1$ NTM at higher pressures approaching the no-wall MHD limit, by using a more sophisticated "target lock" closed-loop feedback scheme to optimize the stabilization, and by elucidating the role of a varying Δ'.

2. Onset Physics

The NTM can spontaneously form when the plasma evolves to a linearly unstable state and a classical island grows, after which the island modifies the equilibrium and transitions to the NTM state and nonlinear instability. It was theoretically predicted that for "classically destabilized" NTMs driven by increasing Δ', the island width evolution should depend upon the rate of approach to the ideal stability boundary [9]. A DIII-D experiment was designed to determine the effect of poles in Δ' on tearing stability in sawtooth-free plasmas by varying $d\beta/dt$ on approach to $m = 2/n = 1$ NTM onset by ramping up the neutral beam injection (NBI) power.

One aim of this work was to study classically-destabilized NTMs in the slow heating regime, where modeling predicts a minimum rate of heating for immediate NTM onset. As the island grows in the slow heating regime, enhanced transport reduces β and Δ' (even considering the increase in heating rate). The combined effects of polarization drift stabilization of a growing island and the reduction of the linear drive due to loss of β and redistribution of current can cause the island to saturate at small levels for low heating rates. Evidence of a lower limit to the heating rate for NTM onset was observed experimentally in DIII-D for the $m = 2/n = 1$ mode, as illustrated in Fig. 1(a,b).

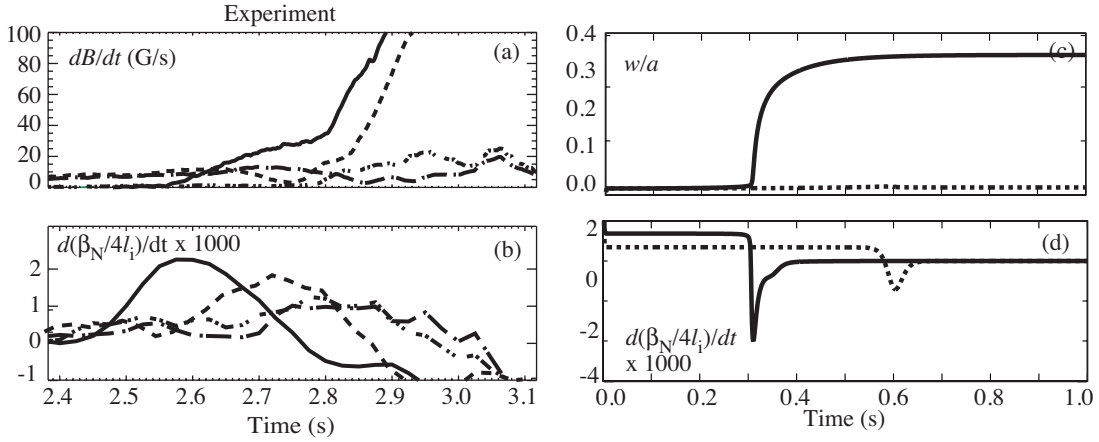

Fig. 1. (a) n=1 Mirnov growth rate, and (b) heating rate for an NBI power scan in DIII-D. In four discharges the rate of change in $d\beta_N/dt$ was decreased sequentially. (c) Normalized island size, determined by integration of the island evolution equation, for two different initial heating rates as shown in (d). Below $d\beta_N/dt = 1.5\text{x}10^{-3}\,s^{-1}$, normalized by $4l_i$, only a small island was observed and no NTM appeared.

We consider a two-level theoretical approach to more fully explore the physics of the above experiment. The first approach is to use the modified Rutherford equation [5,6] to gain insight into how the nonlinear simulations might evolve with time dependent Δ' and β effects. In lieu of a rigorous model for Δ' as a function of island width (w), a linear decrease in Δ' is assumed, $\Delta' = \Delta'_o(\beta) - \alpha_\Delta w$. Here Δ'_o comes directly from a fit to the β dependent linear results from the Pest-III code [10], and α_Δ is chosen such that $\Delta'_o(\beta_{sat}) - \alpha_\Delta w_{sat} \sim -m$ where w_{sat} and β_{sat} are *a priori* estimates on the saturated island width and β during the NTM. Reduction of confinement by enhanced transport at finite island width is implemented

using a linear decrease of the heating rate, $d\beta/dt = d\beta_{heat}/dt - \alpha_H w$. A single α_H is chosen for all rates of heating $d\beta_{heat}/dt$ since the effect of enhanced transport is independent of the heating rate. This yields a model that has $\Delta' \sim -m$ in the large NTM limit and yet responds correctly in the small island regime to the changing linear stability due to $d\beta/dt$.

The modeling begins by increasing β with time toward the ideal MHD limit at the rate $d\beta_{heat}/dt$. Subsequently, Δ' increases and a classical island grows, causing $d\beta/dt$ to be accordingly decreased. For $d(\beta_N/4l_i)/dt < 1.5\text{x}10^{-3}$ s^{-1}, the low heating limit is found and the NTM threshold is not reached as seen in Fig. 1(c,d). The enhanced transport from the classical island reduces β and Δ', and a steady state is found at a small island width below the neoclassical threshold. For $d(\beta_N/4l_i)/dt = 2\text{x}10^{-3}$ s^{-1}, the low heating limit is exceeded and the NTM threshold is surpassed. This simple phenomenological model for the finite island width effects reproduces a reasonable estimate of the heating rate limit when accurate quantities for the parameters are used.

The second theoretical approach uses nonlinear NIMROD simulations in full geometry to give more complete insight into the NTM dependence on the heating rate. This approach includes nonlinear mode coupling but does not incorporate neoclassical effects. Using DIII-D data, a series of equilibria was constructed that increased the pressure multiplicatively while conserving q, as shown in Fig. 2. This mimics the experimental situation even in the low heating regime where the NBI heating was varied on a similar time scale as the island growth rate but still faster than the global current relaxation time. The modeled H-mode pedestal was made slightly broader than the experiment to avoid edge instabilities for large values of β while not altering the local conditions at the $q = 2$ surface. Since the numerical simulations using these equilibria include a vacuum region, making finite edge current intolerable, the pressure-driven and externally-driven current densities are forced to vanish at the separatrix. These equilibria were analyzed first *via* the asymptotic matching method using the PEST-III code. The equilibria show a resistive $m = 2/n = 1$ tearing instability which increases in Δ' and growth rate with pressure, similar to Ref. [9].

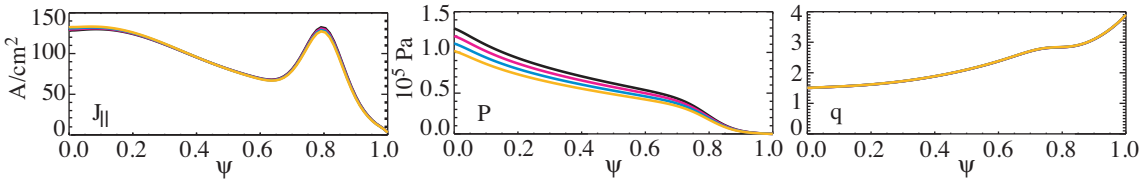

Fig. 2. The model profiles of equilibria based on DIII-D used in the island evolution and numerical simulations. ψ is the normalized poloidal flux.

This series of equilibria were next studied with the NIMROD code, which directly integrates the MHD equations. The linear growth rates calculated by NIMROD, in combination with the Δ' results, are most useful for interpreting the nonlinear results. In the NIMROD analysis, the $m = 2/n = 1$ tearing mode was found to be the most unstable linear mode, and the resultant growth rates as a function β are shown in Fig. 3(a). The instability is increasing in growth rate with increasing β, in agreement with the increase in Δ'.

Using the equilibrium at $\beta_N \sim 1.7$ from Fig. 3(a) as an initial value, simulations with heating were performed to compare with the island evolution equation results and determine how the nonlinear coupling changes the result. The heating is imposed as $P = P_o(1+\gamma t)$, much like the series of equilibria used in the linear studies. The pressure is increased on a time scale much faster than the current relaxation time, $\gamma \sim 200$–400 s^{-1}, therefore the safety factor profile is essentially conserved. These simulations are performed at $S_{sim} \sim 1\text{x}10^6$, and the heating rate is applied at $\gamma \sim (S_{exp}/S_{sim})\gamma_{exp}$ where $S_{sim} \sim 1\text{x}10^8$. Here S is the ratio of the resistive time to the Alfvén time. The experimental $\gamma_{exp} \sim d\beta_N/dt \sim$ 1-10 from Ref. [9]. The instability exhibits super-exponential growth as shown in Fig. 3(b). The simulation shows a $m = 2/n = 1$ mode where the growth rate increases as β is increased. This shows

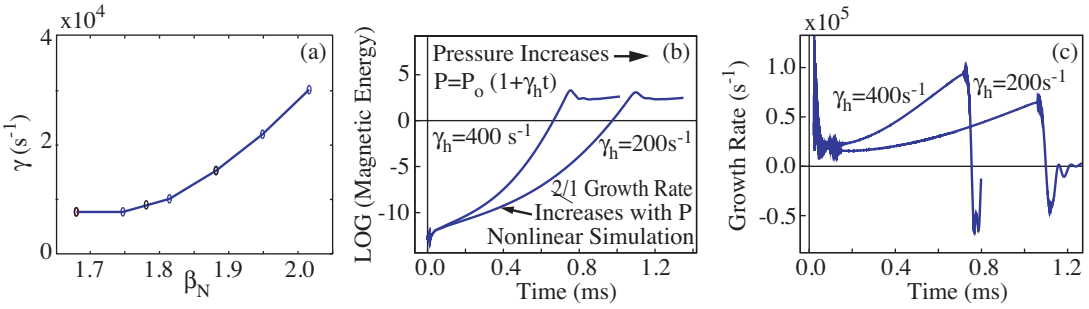

Fig. 3. (a) Linear growth rates *vs*. β_N using NIMROD for a series of equilibria with increasing pressure and constant q, (b) the magnetic energy in the instability as a function of time for the $m = 2/n = 1$ mode in two nonlinear simulations, and (c) the growth rates in those simulations. The increasing pressure from heating causes an increasing growth rate and super-exponential growth.

the MHD linear growth rate is increasing with pressure as predicted by the Δ' and linear NIMROD results. The simulation is essentially modeling the Δ' (β_N) and inner layer effects [11] as well as the nonlinear coupling. However, the neoclassical and two fluid effects are not present; therefore, one does not expect to see evidence of a lull in growth rates as reported in previous work [9], and the island evolution is compared without the neoclassical and two fluid terms.

Looking at the growth rates in Fig. 3(c), it is seen that the lower ramp rate case reaches the same growth rate as the larger ramp rate case in twice the time, or equivalently at the same β. However, the energies in the mode at those times are not at this ratio, but instead the faster heated case has a larger β and larger growth rate at the same energy (or island width) as the lower heated case. This is in agreement with the results of Ref. [9], and can be measured in the experiment. This is true even in the Rutherford regime, where the growth rate increases algebraically, and for any growth rate that is a monotonically increasing function with β. In the experiment, the islands are not detected until they are in the Rutherford regime, and this physical dependence of the growth rate on heating rate at the minimum detected island size determines in part how much ECCD power, for example, will be necessary to stabilize such an island. This is also related to the lower limit in heating rate where the linear drive to the growth rate will be small enough that transport effects cause the island to saturate before reaching the neoclassical threshold. This section demonstrates that the combined employment of analytic, linear computational and nonlinear initial value analysis yields a profound insight into the onset mechanisms of NTMs.

3. Suppression Using ECCD

Complete suppression of the $m = 2/n = 1$ NTM has been achieved in DIII-D using ECCD to replace the "missing" bootstrap current in the island located at the $q = 2$ surface (Fig. 4). An example of this is shown in Fig. 5. These experiments utilized high performance, hybrid-regime discharges [12,13] with closed-loop feedback of the plasma stored energy using the plasma control system (PCS) to control the NBI power. The $m = 2/n = 1$ tearing mode appeared at 3.3 s as indicated by the growing amplitude of the $n = 1$ magnetic fluctuations in

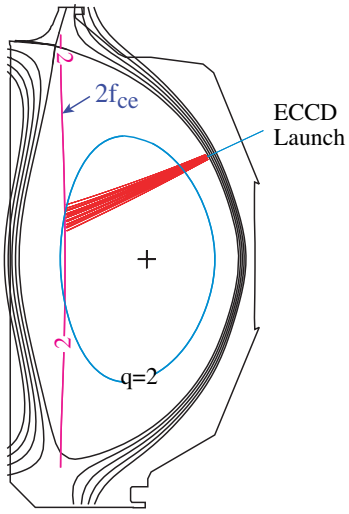

Fig. 4. Cross-section of the plasma equilibrium, the ECCD launch of rays towards the $2f_{ce}$ resonance and the q=2 surface. The rf frequency is 110 GHz and the central toroidal field is 1.55 T.

Fig. 5. (The hybrid regime also has a benign m=3/n=2 NTM that begins early in the discharge.) The unmodulated co-ECCD was injected starting at 4.5 s, driving 37 kA of current at ρ = 0.67 according to the TORAY-GA ray tracing code [14,15]. (ρ is the normalized toroidal flux coordinate.) The amplitude of the m=2/n=1 NTM began to decrease immediately, and after some optimization of the ECCD location (described below) the mode was completely suppressed and did not reappear, even in the presence of sawteeth. ECCD stabilization of the m=2/n=1 NTM was obtained for β_N up to 2.8 ($\beta \leq$ 3.5%), which was equal to 90% of the ideal kink no-wall stability limit ($\approx 4l_i$). This value of β_N is higher than required for the ITER baseline scenario, but it is relevant to advanced tokamak operation in ITER. The NBI power required to maintain constant stored energy decreased by 2.2 MW after ECCD injection owing to island shrinkage and the electron heating from ECCD (albeit far off-axis). Comparing the discharge in Fig. 5 to a lower ECCD power discharge without mode suppression shows that the NTM stabilization resulted in ≈20% improvement (recovery) of the energy confinement time. In lower β_N plasmas, up to 30% improvement in the energy confinement time was observed after m=2/n=1 mode suppression.

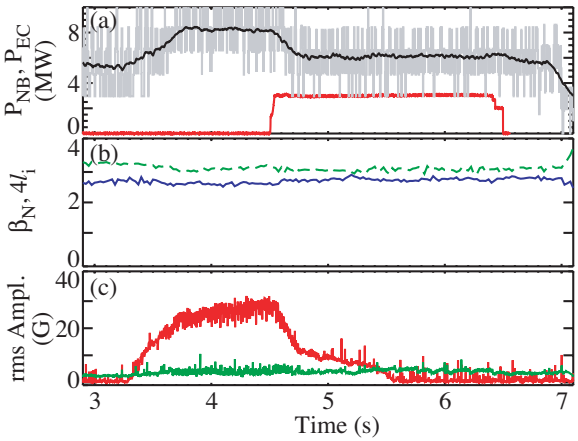

Fig. 5. Time history of #116015 showing (a) NBI (black/grey) and ECCD (red) powers, (b) normalized beta (blue) and ideal no-wall stability limit (dashed green), and (c) rms amplitude of n = 1 (red) and n = 2 (green) tearing modes.

Experiments in DIII-D show that the stabilization of the m = 2/n = 1 NTM was very sensitive to the deposition location [7]. Maximum shrinkage of the island size occurred when the co-ECCD was precisely aligned with the q = 2 surface, the latter location determined from equilibrium reconstructions and fluctuations in the electron cyclotron emission at the island rotation frequency. This agrees with theoretical calculations that show a mismatch of the deposition location from the island on the order of 1–2 cm leads to significant increases in the amount of ECCD required for mode suppression [16]. This motivated development of closed-loop feedback schemes to minimize the ECCD power required to stabilize NTMs. Initial experiments on m = 2/n = 1 mode stabilization in DIII-D used a "search and suppress" algorithm that conducted a blind search to determine the optimal ECCD location. More recent experiments have used a more sophisticated "target lock" algorithm that makes continuous, small variations in B_T to determine the optimal ECCD location at all times. An example of this algorithm for a high β_N discharge is shown in Fig. 6, which plots the trajectory of the n = 1 mode amplitude as a function of the variations in B_T. At the start of ECCD injection, the mode amplitude is 28 G for B_T = 1.555 T. The feedback system first made small B_T variations in each direction throughout the rapid reduction phase, trying to optimize the reduction. This resulted in the mode amplitude decreasing to 11 G for B_T = 1.561 T. As the mode reduction slowed (presumably because the mode width was approaching the ECCD profile width), the feedback system first

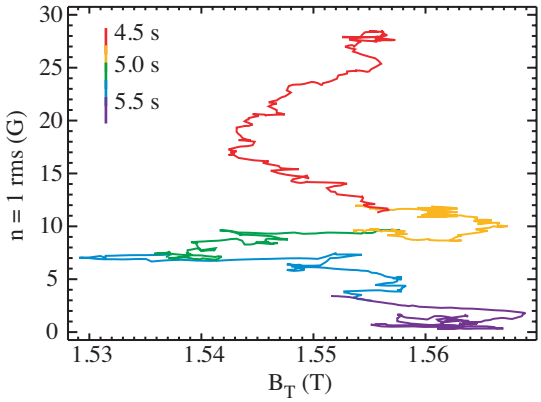

Fig. 6. Trajectory of time history of the n = 1 mode rms amplitude *vs*. the toroidal magnetic field strength selected by the feedback algorithm for #116015. Each color band represents 0.25 s of elapsed time.

tried to lower B_T to 1.530 T, but eventually returned to the original optimum around B_T = 1.562 T. For this magnetic field strength, the m=2/n=1 mode was completely suppressed.

The effects of heating and current drive on the m = 2/n = 1 NTM suppression were separated experimentally by comparing resonance location scans for co, radial, and counter ECCD. The ECCD location was varied using a pre-programmed sweep of B_T from 1.6 T to 1.4 T, which encompassed the optimal value. As seen in Fig. 7 for 2.0 MW of ECCD power, co-injection resulted in the maximum shrinkage of the m = 2/n = 1 island width, while a much smaller island shrinkage was observed for radial injection. The island size increased for counter-injection, leading to a larger loss in confinement. The resonance locations for the maximum effect on the NTM were clearly different for co- and counter-ECCD. Increasing the ECCD power to 3.0 MW resulted in the complete suppression of mode for co-injection, as seen in Fig. 8. For radial injection, the additional ECCD power further shrank the island width but did not lead to full stabilization, while for counter-injection the additional ECCD power increased the island size until the mode locked to the wall and the plasma suffered a minor disruption around 5.0 s.

Modeling of the co/radial/counter ECCD resonance scan using the modified Rutherford equation allows separation of the relative importance between modification of Δ' and driving current within the island. The Rutherford equation can be written in the form

$$\frac{\tau_R}{r}\frac{dw}{dt} = \Delta' r + \frac{128}{3\pi}\frac{J_{BS}}{J_{\|}}\frac{r}{s}\frac{1}{w}\left\{\left[\frac{1}{1+(w_d/w)^2} - \frac{w_{pol}^2}{w^2}\right] \pm K_1 \frac{J_{EC}}{J_{BS}}\right\} \quad , \qquad (1)$$

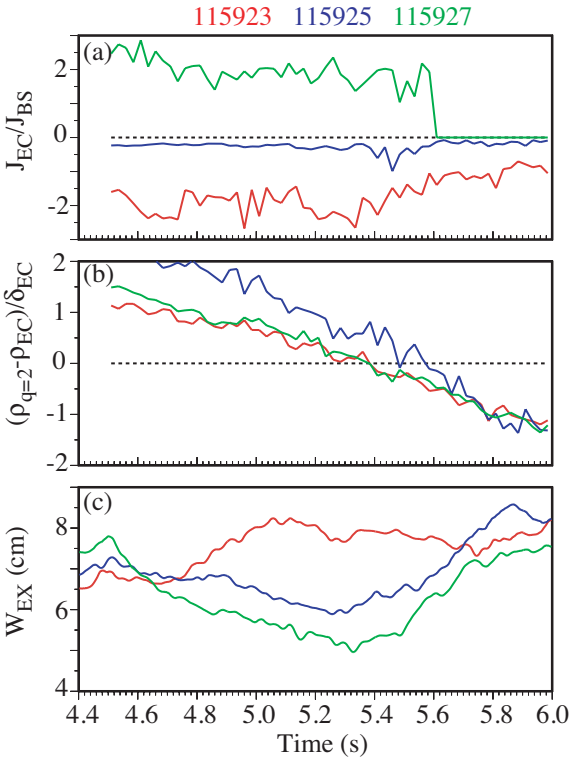

Fig. 7. Resonance position scan for co (green), radial (blue), and counter (red) ECCD with 2.0 MW of injected power: (a) Calculated ratio of driven current density to bootstrap current density, (b) calculated distance between q = 2 surface and ECCD location, normalized to ECCD profile width, and (c) measured m = 2/n = 1 island width.

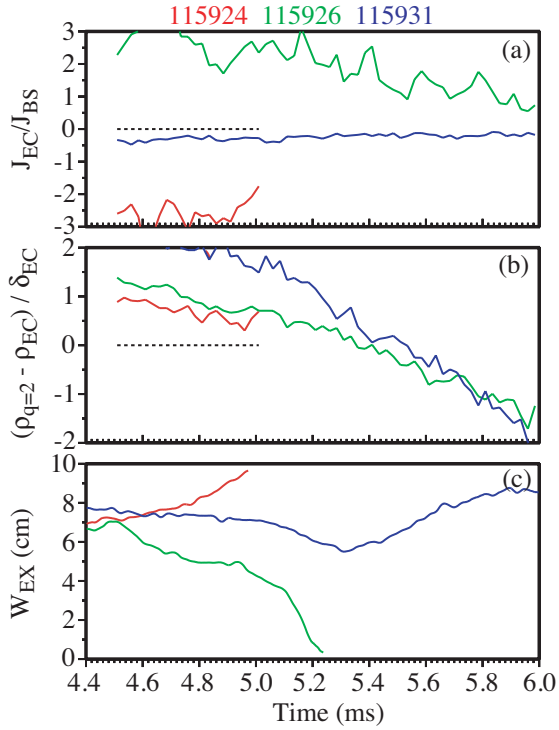

Fig. 8. Resonance position scan for co (green), radial (blue), and counter (red) ECCD with 3.0 MW of injected power: (a) Calculated ratio of driven current density to bootstrap current density, (b) calculated distance between q = 2 surface and ECCD location, normalized to ECCD profile width, and (c) measured m = 2/n = 1 island width.

where the variables are defined in Ref. [16]. The inertia term on the left hand side can be ignored for this slow sweep. The ECCD current density is calculated using TORAY-GA and the time history of the bootstrap current density is determined using experimental profiles. Broadening the ECCD profile by a factor of ≈2.7 compared to TORAY-GA improves the agreement between the model and experiment. There are several possible explanations for this, such as a misalignment between the different ECCD antenna steerings, or radial transport of the current carrying electrons either by the island or by plasma turbulence. Additionally, the model assumes that $\Delta' \propto B_T^2$ to compensate for the change in the safety factor. The magnitude of Δ' was adjusted to best fit the experimental island size on average during each B_T sweep. The model correctly predicts that co-ECCD should shrink the island more than radial injection, with counter-ECCD increasing the island size, as seen by comparing Fig. 9(a) to Fig. 7(c). Using the best fit parameters for the 2.0 MW co-injection case in Fig. 9(a), the model also successfully predicts the time history of a full stabilization discharge with 3.0 MW of co-ECCD power (not shown). The dip in the modeled island width for radial injection is due to a change in the bootstrap current. The best fit value of Δ' is ≈20% smaller (less negative) for counter-ECCD compared to co-ECCD for the 2.0 MW case, whereas the island size changed by a factor of 1.5. For the 3.0 MW ECCD case, the value of Δ' determined by fitting Eq. (1) to experiment is ≈40% smaller for counter-injection compared to co-injection. This indicates that the change in linear stability had a significant effect on the island width during ECCD, although the current drive effect in the island O-point was probably the dominant factor. Furthermore, the residual between the modeled and measured m=2/n=1 island widths, shown in Fig. 9(b), indicates that Δ' may have been changing dynamically during the B_T scan by an additional ≈10%. This dynamic variation in Δ' appears to be symmetric about the optimal point for co-injection and asymmetric for counter-injection, which is not predicted theoretically [17].

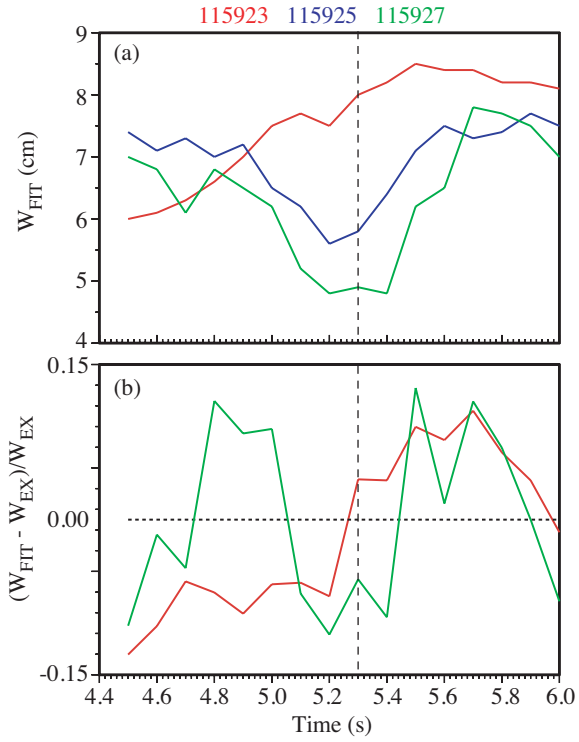

Fig. 9. (a) Modeled island widths during B_T scan shown in Fig. 6 for co (green), radial (blue), and counter (red) ECCD. (b) Residual between modeled and measured m = 2/n = 1 island widths.

4. Conclusions

A series of DIII-D experimental cases that exemplified the onset and evolution physics of classically-destabilized m = 2/n = 1 NTMs was compared to analytic and numerical limits on the rate of change in β as the ideal MHD limit was approached. These simulations clearly reproduced the evolving linear instability drive from the island evolution equation, confirming the validity of the theory and suggesting this effect should be observed in experiment. No asymptotic matching condition with an inner layer or Rutherford assumption was used, as is the case in linear growth rate and island evolution analyses. Instead the full MHD equations were integrated, giving credence to the validity of the island evolution result. Comparison of co/radial/counter ECCD near the island location for the m = 2/n = 1 NTM showed clearly co-ECCD was the most effective for stabilization. In addition to replacing the "missing" bootstrap current, ECCD appeared to cause a change in the linear stability that

helped to shrink the island for co-injection. Using a closed-loop feedback scheme to determine the optimal ECCD location at all times, the $m = 2/ n= 1$ NTM was completely suppressed in plasmas with β_N up to 2.8 ($\beta \leq 3.5\%$), which was equal to 90% of the ideal no-wall MHD limit. The demonstration of the complete suppression of the $m = 2/n = 1$ NTM using ECCD at the $q = 2$ surface improves confidence that a control system to prevent confinement loss and disruptions arising from this mode can be developed in ITER.

Acknowledgments

This is a report of work supported by the U.S. Department of Energy under DE-FC02-04ER54698, DE-AC05-76OR00033, DE-AC02-76CH03073, and DE-AC05-00OR22725.

References

[1] FURTH, H.P., *et al*., Phys. Fluids **6** (1963) 459.
[2] RUTHERFORD, P.H., Phys. Fluids **16** (1973) 1903.
[3] CARRERA, R., *et al*., Phys. Fluids **29** (1986) 899.
[4] CHANG, Z., *et al*., Phys. Rev. Lett. **74** (1995) 4663.
[5] HEGNA, C.C., and CALLEN, J.D., Phys. Plasmas **4** (1997) 2940.
[6] ZOHM, H., Phys. Plasmas **4** (1997) 3433.
[7] PETTY, C.C., *et al*., Nucl. Fusion **44** (2004) 243.
[8] GANTENBEIN, G., *et al*., Proc. 30th Euro. Conf. on Controlled Fusion and Plasma Physics (St Petersburg, 2003) Vol. 27A (Geneva: EPS) p. P1.187.
[9] BRENNAN, D.P., *et al*., Phys. Plasmas **10** (2003) 1643.
[10] LUTJENS, H., *et al*., Phys. Plasmas **9** (2002) 219.
[11] GLASSER, A.H., GREENE, J.M., and JOHNSON, J.L., Phys. Fluids **18** (1975) 875.
[12] WADE, M.R., *et al*., Phys. Plasmas **8** (2001) 2208.
[13] LUCE, T.C., *et al*., Nucl. Fusion **41** (2001) 1585.
[14] MATSUDA, K., IEEE Trans. Plasma Sci. **17** (1989) 6.
[15] LIN-LIU, Y.R., *et al.,* Phys. Fluids **10** (2003) 4064.
[16] PRATER, R., *et al*., Nucl. Fusion **43** (2003) 1128.
[17] WESTERHOF, E., Nucl. Fusion **30** (1990) 1143.